Thin-film Josephson junctions with alternating critical current density

Maayan Moshe,[1] V. G. Kogan,[2] and R. G. Mints[1,*]
[1]*The Raymond and Beverly Sackler School of Physics and Astronomy, Tel Aviv University, Tel Aviv 69978, Israel*
[2]*Department of Physics and Astronomy and Ames Laboratory–DOE, Iowa State University, Ames, Iowa 50011, USA*
(Received 15 October 2008; published 13 January 2009)

We study the field dependence of the maximum current $I_m(H)$ in narrow edge-type thin-film Josephson junctions with alternating critical current density. $I_m(H)$ is evaluated within nonlocal Josephson electrodynamics taking into account the stray fields that affect the difference of the order-parameter phases across the junction and therefore the tunneling currents. We find that the phase difference along the junction is proportional to the applied field, depends on the junction geometry, but is independent of the Josephson critical current density g_c, i.e., it is universal. An explicit form for this universal function is derived for small currents through junctions of the width $W \ll \Lambda$, the Pearl length. The result is used to calculate $I_m(H)$. It is shown that the maxima of $I_m(H) \propto 1/\sqrt{H}$ and the zeros of $I_m(H)$ are equidistant but only in high fields. We find that the spacing between zeros is proportional to $1/W^2$. The general approach is applied to calculate $I_m(H)$ for a superconducting quantum interference device with two narrow edge-type junctions. If g_c changes sign periodically or randomly, as it does in grain boundaries of high-T_c materials and superconductor-ferromagnet-superconductor heterostructures, $I_m(H)$ not only acquires the major side peaks, but due to nonlocality the following peaks decay much slower than in bulk junctions.

DOI: 10.1103/PhysRevB.79.024505 PACS number(s): 74.50.+r, 74.72.−h

I. INTRODUCTION

The edge-type thin-film Josephson junctions (see Fig. 1) in magnetic fields behave differently from junctions between bulk superconductors. The difference is caused mainly by the stray fields outside the film. Indeed, since there is no typical length scale for the fields *outside* the junction, the stray fields strongly affect the screening and tunneling *through* the junction at all distances. As a result, the drop of the order-parameter phase φ across the superconducting banks is defined by an integral equation.[1–8] The kernel of this equation depends on the tunneling characteristics and on the spatial distribution of the stray fields at the film surfaces. In other words, electrodynamics in edge-type thin-film Josephson junctions is *nonlocal*.

Studies of edge-type thin-film Josephson junctions took off after the discovery of anomalous electromagnetic properties of Josephson grain boundaries in thin films of high-T_c superconductors.[9–13] It was established experimentally that the joint effect of meandering grain boundaries and of the d-wave symmetry of the order-parameter results in appearance of nearly periodic sequences of interchanging 0- and π-shifted Josephson junctions along the boundary.[9–13] In other words, the Josephson critical current density alternates along these grain boundaries.[14–16] Similar critical current density alternations were found recently in superconductor-ferromagnet-superconductor heterostructures[17–22] and zigzag-type junctions between high- and low-T_c superconductors.[16] The spatial distributions of fields and currents in these junctions are affected by the stray fields and vice versa. This results in appearance of complex dependencies of the maximum current I_m on the applied field H. The theory of the patterns $I_m(H)$ for the edge-type thin-film Josephson junctions with alternating critical sheet current density is just emerging.

In edge-type thin-film junctions the length scale ℓ of spatial variations in the phase difference is given by

$$\ell = \frac{c\phi_0}{8\pi^2 \Lambda \langle g_c \rangle}, \tag{1}$$

where $\Lambda = 2\lambda^2/d$ is the Pearl length, λ is the London penetration depth $\lambda \gg d$, d is the film thickness, and the average critical sheet current density $g_c(y)$ is defined as

$$\langle g_c \rangle = \int_{-W/2}^{W/2} g_c(y) \frac{dy}{W}. \tag{2}$$

It is worth mentioning that in edge-type junctions ℓ is the length scales for current and field variations *along* the junction, whereas Λ is the scale for these variations in the *transverse* direction. For the bulk junctions with a standard (local) Josephson electrodynamics, these length scales are given by the Josephson length $\lambda_J = (c\phi_0/16\pi^2 j_c \lambda)^{1/2}$ and the London penetration depth λ.[23,24]

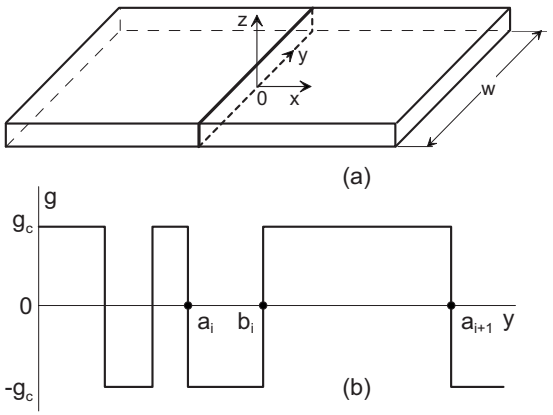

FIG. 1. (a) Sketch of an edge-type Josephson junction in a thin-film strip; the junction plane is shown by the dotted cross section. (b) Spatially alternating critical sheet current $g_c(y)$ in a sequence of 0 and π biased Josephson junctions.

The formal method of our analysis has been described in a short Ref. 8 where we have shown that if the length ℓ exceeds both the junction width W and the Pearl Λ, the phase difference $\varphi(y)$ for small currents is the same for junctions with different Josephson critical currents, i.e., $\varphi(y)$ is a material independent *universal* function; it depends only on the applied field and the junction length.

We have evaluated the field dependence of the maximum supercurrent $I_m(H)$ through the junction that turns out to be quite different from the standard Fraunhofer pattern of bulk junctions. Zeros of $I_m(H)$ become equidistant only in large fields, and are separated by $\Delta H \sim \phi_0/W^2$, which is much smaller than $\phi_0/W\lambda$ of bulk junctions of the same length. The maxima of $I_m(H)$ decrease as $1/\sqrt{H}$, which is slower than $1/H$ for the bulk. We have shown that $I_m(H)$ for a superconducting quantum interference device (SQUID) made of narrow thin-film strips with edge-type junctions differ remarkably from the canonic Fraunhofer pattern.

In this paper, we expand the approach developed in Ref. 8 and apply it to treat Josephson junctions with critical current density spatially alternating along the junction. In particular, this is the case of faceted grain boundaries in YBCO films,[9–12] superconductor-ferromagnet-superconductor heterostructures,[17–22] and zigzag-type junctions between high- and low-T_c superconductors.[16] Our calculations of $I_m(H)$ reproduce major features of experimental results.

The paper is organized as follows, In Sec. II, we describe the method in Ref. 8 and reproduce major results for the straight edge-type junction in thin-film strips with $W < \{\ell, \Lambda\}$ and a uniform critical current. We consider effects imposed by periodic and random alternations of $g_c(y)$ on the patterns $I_m(H)$. We demonstrate by numerical calculations the typical fingerprints of nonlocal Josephson electrodynamics. Smearing of the typical structure of peaks in the dependence $I_m(H)$ is considered. In Sec. III, we apply the approach developed to treat a model rectangular SQUID of two narrow thin-film edge-type Josephson junctions. A summary concludes the paper.

II. JUNCTION IN NARROW STRIPS

A. Constant critical current density

We begin from the case when the Josephson critical current density is constant along the junction. Since div $\boldsymbol{g}=0$, the sheet current density $\boldsymbol{g}=(g_x, g_y)$ in thin films can be written as $\boldsymbol{g}=\text{curl}\, S\hat{z}=(\partial_y S, -\partial_x S)$, where $S(x,y)$ is the stream function. The sheet current normal to the strip edges ($y = \pm W/2$) is zero, i.e., $S(x, \pm W/2)$ are constants. The total current through the strip is

$$I = \int_{-W/2}^{W/2} g_x dy = S\left(\frac{W}{2}\right) - S\left(-\frac{W}{2}\right). \tag{3}$$

Integrating London equations over the film thickness we obtain

$$h_z + \frac{2\pi\Lambda}{c}\text{curl}_z\, \boldsymbol{g} = \frac{\phi_0}{2\pi}\delta(x)\varphi'(y), \tag{4}$$

where h_z consists of the applied field H and the part related to $\boldsymbol{g}$ by the Biot-Savart integral. The right-hand side here (Appendix A) is a manifestation of a general rule: the field of a Josephson junction is formally equivalent to the field of a set of vortexlike singularities distributed along the junction with the line density $\varphi'(y)/2\pi$.[5,7]

In strips with $W \ll \Lambda$, the self-field of the current $\boldsymbol{g}$ is of the order g/c, whereas the second term on the left-hand side of Eq. (3) is of the order $g\Lambda/cW \gg g/c$. Hence, the self-field can be disregarded, unlike the *applied* field H. Substituting $\text{curl}_z\, \boldsymbol{g} = -\nabla^2 S$ in Eq. (4) one obtains

$$\frac{2\pi\Lambda}{c}\nabla^2 S = -\frac{\phi_0}{2\pi}\delta(x)\varphi'(y) + H. \tag{5}$$

This *linear* equation has solutions $S = S_1 + S_2$ such that

$$\frac{2\pi\Lambda}{c}\nabla^2 S_1 = -\frac{\phi_0}{2\pi}\delta(x)\varphi'(y), \tag{6}$$

$$\frac{2\pi\Lambda}{c}\nabla^2 S_2 = H. \tag{7}$$

Boundary condition (3) is satisfied if $S_1(\pm W/2)=0$ and $S_2(W/2) - S_2(-W/2) = I$.

Hence, we have

$$S_1(\boldsymbol{r}) = \int d\boldsymbol{\rho}\,\delta(u)\frac{\varphi'(v)}{2\pi}G(\boldsymbol{r},\boldsymbol{\rho}), \tag{8}$$

where $\boldsymbol{r}=(x,y)$ and $\boldsymbol{\rho}=(\tilde{x},\tilde{y})$. Green's function $G(\boldsymbol{r},\boldsymbol{\rho})$ satisfies the equation

$$\frac{2\pi\Lambda}{c\phi_0}\nabla^2 G = -\delta(\boldsymbol{r}-\boldsymbol{\rho}) \tag{9}$$

with zero boundary conditions[25]

$$G = \frac{c\phi_0}{4\pi^2\Lambda}\tanh^{-1}\frac{\cos X \cos\tilde{X}}{\cosh(Y-\tilde{Y}) - \sin X \sin\tilde{X}}, \tag{10}$$

where the capitals stand for corresponding coordinates in units of W/π. In fact, $G(\boldsymbol{r},\boldsymbol{\rho})$ gives the current distribution of a single vortex at the point $\boldsymbol{\rho}$ of a narrow strip. Clearly, S_1 describes the current perturbation due to the junction.

We further obtain

$$S_2(\boldsymbol{r}) = \frac{cH}{4\pi\Lambda}y^2 + \frac{I}{W}y. \tag{11}$$

The first term here represents the screening currents due to the applied field, whereas the second is due to a uniform transport current.

Given the stream function we write the current through the junction $g_x(0,y) = g_c \sin\varphi(y) = \partial_y S(0,y)$. This results in the integral equation for the phase $\varphi(y)$,

$$\frac{W}{\ell}\sin\varphi - i = \int_{-\pi/2}^{\pi/2} d\tilde{Y}\frac{\varphi'(\tilde{Y})\cos\tilde{Y}}{\sin\tilde{Y} - \sin Y} + hY, \tag{12}$$

where

$$h = \frac{4W^2}{\phi_0} H, \quad i = \frac{8\pi^2 \Lambda}{c\phi_0} I \tag{13}$$

are the characteristic length, reduced field, and reduced total current.

The boundary conditions for $\varphi(y)$ follow from the London equation for $g_y(\pm 0, y)$ on the two junction banks,

$$g_y(\pm 0, y) = -\frac{c\phi_0}{4\pi^2 \Lambda}\left[\frac{\partial \theta(\pm 0, y)}{\partial y} - \frac{2\pi}{\phi_0} A_y\right], \tag{14}$$

where $\theta(x,y)$ is the phase and $\boldsymbol{A}$ is the vector potential. We subtract these equations and utilize the continuity of $\boldsymbol{A}$ to obtain $\varphi'(y) \propto g_y(0,y)$. The current g_y must vanish at the junction edges, i.e., the boundary conditions for $\varphi'(y)$ are given by

$$\varphi'(-W/2) = \varphi'(W/2) = 0. \tag{15}$$

A remarkable feature of narrow ($W \ll \Lambda$) junctions is to be noticed: the length ℓ along with g_c, the material parameter of the junction, enter only the left-hand side of Eq. (12). If $W \ll \ell$, or which is the same $g_c \ll c\phi_0 / 8\pi^2 \Lambda^2$, the left-hand side can be disregarded leaving an equation for φ with no material parameters,

$$\int_{-\pi/2}^{\pi/2} d\tilde{Y} \varphi'(\tilde{Y}) \frac{\cos \tilde{Y}}{\sin \tilde{Y} - \sin Y} + hY = 0. \tag{16}$$

In turn this means that the phase difference is just proportional to the applied field h. Writing $\varphi'(Y) = h\varphi_0'(Y)$ we obtain for the function $\varphi_0'(Y)$ an equation that does not contain any physical parameters,

$$\int_{-\pi/2}^{\pi/2} d\tilde{Y} \varphi_0'(\tilde{Y}) \frac{\cos \tilde{Y}}{\sin Y - \sin \tilde{Y}} = -Y, \tag{17}$$

and therefore $\varphi_0'(Y)$ is a *universal* function.

Equation (17) with boundary conditions [Eq. (15)] can be solved exactly (see Appendixes B and C),

$$\varphi_0'(Y) = \frac{1}{\pi^2 \cos Y}\left(2 - \int_{-\pi/2}^{\pi/2} \frac{\tilde{Y} \cos^2 \tilde{Y} d\tilde{Y}}{\sin Y - \sin \tilde{Y}}\right). \tag{18}$$

The integral here is understood as Cauchy principal value and can be done numerically. However, its value at the strip middle is found exactly: $\varphi_0'(0) = 4\beta(2)/\pi^2 \approx 0.371$, where $\beta(2)$ is Catalan's constant. The universal function $\varphi_0'(Y)$ calculated numerically is shown in Fig. 2(a). The function $\varphi_0(Y)$ obtained requiring it to be odd in Y is shown in Fig. 2(b). In particular, this calculation gives $\varphi_0(\pi/2) - \varphi_0(-\pi/2) \approx 0.86$.

We thus obtain for narrow thin-film junctions,

$$\varphi(Y) = h\varphi_0(Y) + \eta \tag{19}$$

with an arbitrary constant η. The total current through the junction is

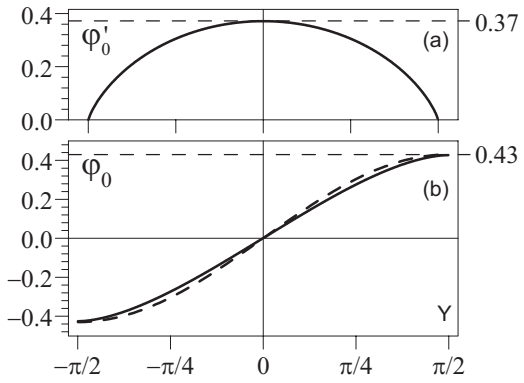

FIG. 2. (a) The function $\varphi_0'(Y)$ calculated according to Eq. (18). (b) The solid line is $\varphi_0(Y)$ obtained by numerical integration of $\varphi_0'(Y)$ shown in the panel (a). The dashed line is the approximation $\varphi_0 = 0.43 \sin Y$.

$$I = \frac{g_c W}{\pi} \int_{-\pi/2}^{\pi/2} dY \sin[h\varphi_0(Y) + \eta]. \tag{20}$$

Maximizing I with respect to η provides $\eta = \pi/2$ and the maximum current I_m,

$$\frac{I_m}{g_c W} = \frac{2}{\pi}\left|\int_0^{\pi/2} dY \cos[h\varphi_0(Y)]\right|. \tag{21}$$

Hence, $I_m(H)$ can be evaluated numerically; the result is shown as a solid line in Fig. 3.

A good approximation for $I_m(H)$ can be obtained as follows. The odd function $\varphi_0(Y)$ can be written as the Fourier series $\Sigma a_n \sin(2n+1)Y$ to satisfy boundary conditions [Eqs. (15)]. We take the lowest approximant

$$\varphi_0 = a_0 \sin Y \tag{22}$$

with $a_0 = 0.43$ to fit the difference $\varphi_0(\pi/2) - \varphi_0(-\pi/2) = 0.86$ that is found numerically. The panel (b) in Fig. 2 shows that this approximation is close to the phase found numerically (see Appendix C).

Using Eq. (22) we have

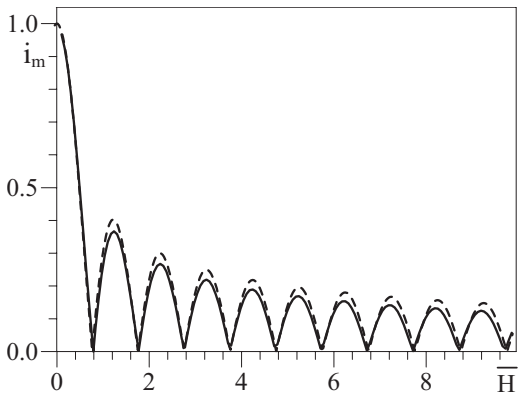

FIG. 3. The maximum supercurrent $i_m = I_m / g_c W$ versus the normalized applied field $\bar{H} = 4a_0 W^2 H / \pi\phi_0$. The dashed line is approximation (20).

$$\frac{I_m}{g_c W} = \frac{2}{\pi}\left|\int_0^{\pi/2} dY \cos(ha_0 \sin Y)\right| = |J_0(a_0 h)|. \quad (23)$$

Figure 3 shows that this approximation is quite accurate as compared to $I_m(H)$ calculated numerically with the help of Eq. (21). Zeros of the Bessel function $J_0(x)$ are equidistant for large arguments, but they are spaced roughly by π everywhere. Hence zeros of $I_m(h)$ are separated by $a_0\Delta h \simeq \pi$ or in common units by

$$\Delta H \simeq 1.8\frac{\phi_0}{W^2}. \quad (24)$$

It is worth recalling that in bulk junctions of the length W the zeros are separated by $\Delta H \approx 2\phi_0/W\lambda$ that exceeds by much the thin-film spacing. A similar purely numerical estimate is given in Ref. 2.

In the high-field region one can use the large argument asymptotics of $J_0(x)$ to obtain

$$I_m \approx 0.61 g_c \sqrt{\frac{\phi_0}{H}}\left|\cos\left(1.72\frac{HW^2}{\phi_0} - \frac{\pi}{4}\right)\right|. \quad (25)$$

Thus, the maxima of $I_m(H)$ decrease as $1/\sqrt{H}$, i.e., slower than in the bulk case where $I_m \propto 1/H$.

It is worth noting that in high fields the maxima of $I_m(H)$ do not depend on the junction length W. Qualitatively, this comes about because the tunneling current $g_x = g_c \sin(h\varphi_0 + \theta)$ oscillates fast for $h \gg 1$ so that most of the junction length does not contribute to the total current, unlike the narrow belts of the width $\delta \sim \sqrt{\phi_0/H}$ near the strip edges.

In practice the pattern shown in Fig. 3 might be distorted by Pearl vortices trapped in the junction banks. The energy of these vortices[26–29] acquires a minimum in the strip middle starting from fields of the order ϕ_0/W^2. However, estimates of the energy ϵ_J of Josephson vortices as compared to Pearl ones, ϵ_P, yield $\epsilon_J/\epsilon_P \sim 0.1/\ln(2W/\xi)$, where ξ is the coherence length and $\ln(2W/\xi)$ is large. Physically, this makes the Josephson contact a "weak spot" where vortices penetrate the sample first. Hence the chances are good for recording quite a few maxima of $I_m(H)$ provided the strip is homogeneous and the pinning is weak.

B. Spatially varying critical current density

When the critical sheet current density varies along the junction the maximum supercurrent is given by

$$I_m = \frac{W}{\pi}\max\left|\int_{-\pi/2}^{\pi/2} dY g_c(Y)\sin(a_0 h \sin Y + \eta)\right|. \quad (26)$$

To demonstrate the basic features imposed upon the patterns $I_m(H)$ by the coordinate dependence of $g_c(y)$, we use a stepwise model for $g_c(y)$ suggested in Ref. 30 and shown in Fig. 1(b). $g_c(y)$ is assumed to take positive and negative values in N interchanging intervals or "facets,"

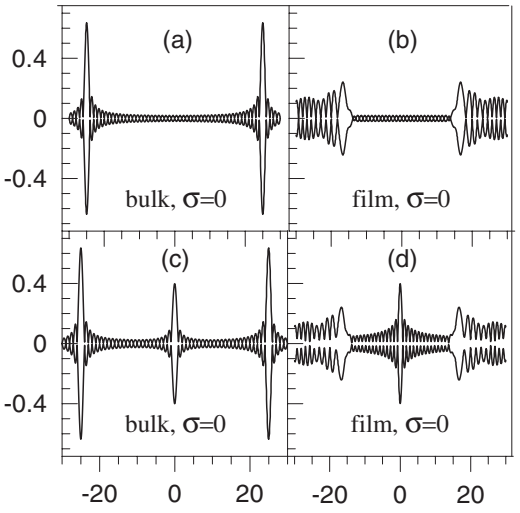

FIG. 4. The maximum supercurrent $i_m = I_m/g_c W$ versus normalized applied field $\bar{H} = 4a_0 W^2 H/\pi\phi_0$ for thin-film junctions and versus $\bar{H} = 2\lambda WH/\phi_0$ for bulk junction with 50 periodically spaced facets. Panels (a) and (b) are for $\langle g_c\rangle = 0$, whereas panels (c) and (d) are for $\langle g_c\rangle = 0.4g_0$. Calculations are performed using the local Josephson electrodynamics for the bulk case and the nonlocal one for films.

$$g_c(y) = g_0\begin{cases} 1, & a_i < y < b_i \\ -1, & b_i < y < a_{i+1}, \end{cases} \quad (27)$$

$i = 1, 2, \ldots, N/2$. Thus, $g_c = g_0$ within $N/2$ facets with lengths $l_i^+ = b_i - a_i$ and $g_c = -g_0$ within $N/2$ facets with lengths $l_i^- = a_{i+1} - b_i$.

Two options are considered: *periodic* structures with $l_i^+ = l_i^- = l = W/N$ and *random* ones with the lengths l_i^+ and l_i^- randomly distributed around the length l. The randomness is characterized by the standard deviation,

$$\sigma = \frac{1}{l}\left\{\frac{1}{N}\sum_{i=1}^{N/2}[(l_i^+ - l)^2 + (l_i^- - l)^2]\right\}^{1/2} \quad (28)$$

and by the average critical current $\langle g_c\rangle$ defined in Eq. (2). We have evaluated numerically the maximum current $I_m(H)$ and show the results in Figs. 4–6.

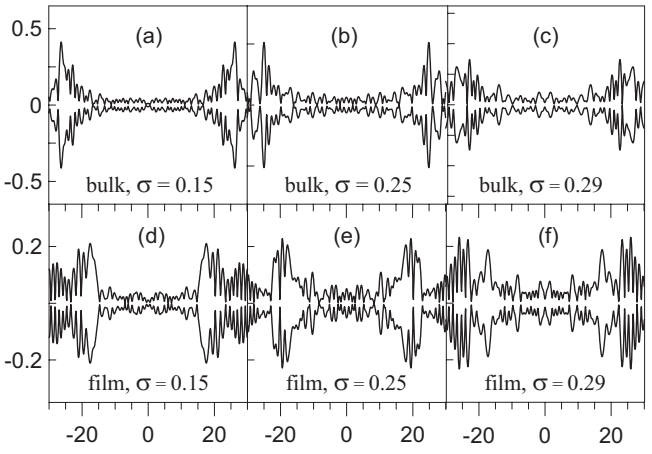

FIG. 5. The same as Fig. 4 for $\langle g_c\rangle = 0$ and for the standard deviations from periodicity σ indicated in the panels.

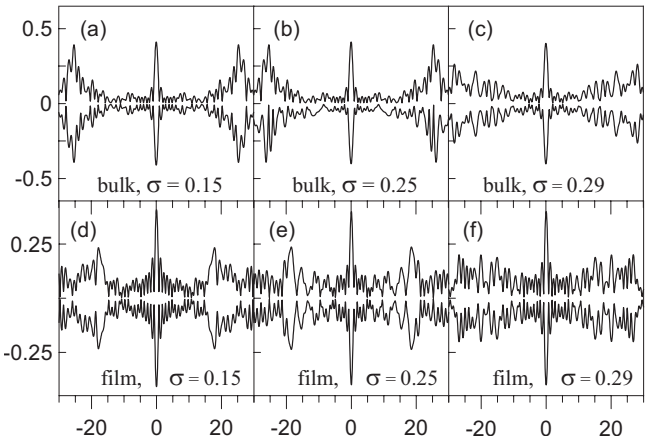

FIG. 6. The same as Fig. 4 for $\langle g_c \rangle = 0.4 g_0$ and for the standard deviations from periodicity σ indicated in the panels.

For a periodic $g_c(y)$, $\sigma=0$. The fingerprints of this periodicity for the situation with $\langle g_c \rangle = 0$ are the absence of the central peak at $H=0$ and the presence of side peaks in patterns $I_m(H)$. For the bulk junctions, this pattern, considered in Ref. 30, is shown in panel (a) of Fig. 4. As is shown in the panel (b), these features of the g_c periodicity are still present for the edge-type thin-film junction. However, the differences brought by the nonlocality are evident not only in the different pattern of $I_m(H)$ between the side peaks but also in a much slower decay of maxima following the major side peaks.

The panels (c) and (d) of Fig. 4 show the results of the same calculation for the bulk and thin-film junctions for $\sigma = 0$ and $\langle g_c \rangle = 0.4 g_0$. Again, the nonlocality causes a much slower decay of the pattern maxima.

Deviations from the periodicity of $g_c(y)$ smear the peaks; examples are shown in Figs. 5 and 6 and are compared to patterns obtained using the local Josephson electrodynamics for bulk junctions. Relevance of these examples comes out clearly if one compares the calculated patterns of $I_m(H)$ with the experimental data in Ref. 16: qualitatively calculated $I_m(H)$ is similar to experimental patterns.

III. RECTANGULAR SQUID

Let us consider now current flowing through rectangular SQUID made of narrow thin-film strips with two identical junctions sketched in Fig. 7. In zero field the current distribution is symmetric with respect to the SQUID center and the line integral of $\boldsymbol{g}$ along any symmetric contour is zero.

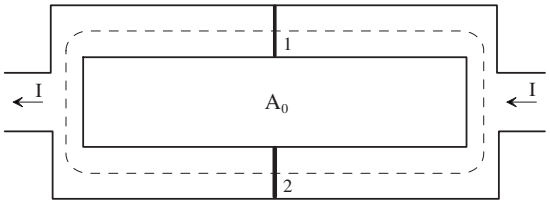

FIG. 7. Sketch of a rectangular SQUID made of two narrow thin-film strips with identical edge-type junctions 1 and 2.

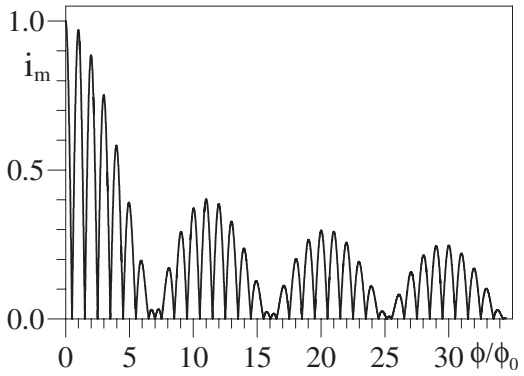

FIG. 8. The maximum supercurrent $i_m = I_m / 2 g_c W$ versus flux ϕ/ϕ_0 for a rectangular SQUID (Fig. 4) with $A_0/W^2 = 5$.

When the field is applied, this symmetry is violated by the screening currents. However, at the contour in the strips, middle (shown in the figure), the screening currents vanish so that the contour integral of $\boldsymbol{g}$ remains zero. This contour crosses the junctions at their middle. The flux ϕ enclosed by this contour does not change if the contour is shifted as a whole by Y. Integrating the London equation for $\mathbf{g}$ over such a contour we obtain

$$\varphi_2(Y) - \varphi_1(Y) = 2\pi\phi/\phi_0 \tag{29}$$

(the coordinate Y is counted in each strip from its middle).

The total current through the system is given by

$$\frac{\pi I}{g_c W} = \int_{-\pi/2}^{\pi/2} dY (\sin\varphi_1 + \sin\varphi_2) = 2\int_{-\pi/2}^{\pi/2} dY \sin\left(ha_0 \sin Y + \eta + \frac{\pi\phi}{\phi_0}\right)\cos\frac{\pi\phi}{\phi_0}, \tag{30}$$

where η is a constant. The maximum current corresponds to $\eta = \pi/2 - \pi\phi/\phi_0$ (see Fig. 8),

$$I_m = 2 g_c W \left| J_0\left(4a_0 \frac{W^2}{A_0}\frac{\phi}{\phi_0}\right)\cos\frac{\pi\phi}{\phi_0}\right|, \tag{31}$$

where A_0 is the area of the "central" contour. Note that Eq. (31) is valid if $L \gg W$ (see Fig. 4).

An example of $I_m(\phi/\phi_0)$ is shown in Fig. 5 for a SQUID with $A_0/W^2 = 5$. The standard SQUID pattern $|\cos(\pi\phi/\phi_0)|$ is modulated in our case by a slow varying Bessel function. We stress again that the pattern shown is obtained for large area SQUIDs with two narrow thin-film junctions; for reduced areas the interference patterns become more complex, a subject for further study.

IV. SUMMARY

To summarize, we have evaluated the field dependence of the maximum supercurrent in narrow edge-type Josephson junctions in thin-film strips; the strip width W is supposed to be less than the Pearl length Λ and the thin-film Josephson length ℓ of Eq. (1). Calculations are done in the framework

of nonlocal Josephson electrodynamics. We demonstrate that the stray fields cause a pattern $I_m(H)$ with much reduced distance between zeros, $\Delta H \sim \phi_0/W^2$, and with a slow decreasing maxima in high fields, $I_m(H) \propto 1/\sqrt{H}$. The flux dependence of the maximum supercurrent through a SQUID made of narrow thin-film strips with edge-type junctions differs by much from the standard periodicity. If the Josephson critical current changes sign periodically or randomly, as it does in grain boundaries of high-T_c materials and superconductor-ferromagnet-superconductor heterostructures, $I_m(H)$ not only acquires the major side peaks, but due to nonlocality the following peaks decay much slower than in bulk junctions in qualitative agreement with existing data.

ACKNOWLEDGMENTS

The authors are grateful to D. J. Van Harlingen, A. Gurevich, J. Mannhart, and C. Schneider for stimulating discussions. The work of V.G.K. at Ames Laboratory is supported by the Office of Basic Energy Sciences of the U.S. Department of Energy under Contract No. DE-AC02-07CH11358.

APPENDIX A

The London equation everywhere on the film except the junction reads

$$h_z + \frac{2\pi\Lambda}{c}\mathrm{curl}_z\, \mathbf{g} = 0, \quad x \neq 0. \tag{A1}$$

At the junction line $x=0$, the current component g_y is discontinuous. One can write for the whole x, y plane,

$$h_z + \frac{2\pi\Lambda}{c}\mathrm{curl}_z\, \mathbf{g} = f(y)\,\delta(x), \tag{A2}$$

where the function $f(y)$ is to be determined. To this end, integrate Eq. (A2) over the area within the contour following the junction banks along $x=\pm 0$ and crossing the junction at y_1 and y_2. The magnetic flux through this contour is zero, and we obtain

$$\frac{2\pi\Lambda}{c}\int_{y_1}^{y_2}[g_y(+0,y) - g_y(-0,y)]dy = \int_{y_1}^{y_2} f(y)dy \tag{A3}$$

for any y_1 and y_2. This gives

$$\frac{2\pi\Lambda}{c}[g_y(+0,y) - g_y(-0,y)] = f(y). \tag{A4}$$

Use the London relation

$$\mathbf{g} = -\frac{c\phi_0}{4\pi^2\Lambda}\left(\nabla\theta + \frac{2\pi}{\phi_0}\mathbf{A}\right) \tag{A5}$$

and the definition of the gauge-invariant phase difference

$$\varphi(y) = \theta(-0,y) - \theta(+0,y) - \frac{2\pi}{\phi_0}\int_{-0}^{+0} dx A_x(x,y) \tag{A6}$$

to obtain

$$\frac{d\varphi}{dy} = \frac{4\pi^2\Lambda}{c\phi_0}[g_y(+0,y) - g_y(-0,y)]. \tag{A7}$$

Equations (A4) and (A7) yield

$$f(y) = \frac{\phi_0}{2\pi}\varphi'(y). \tag{A8}$$

APPENDIX B

To determine $\varphi_0'(Y)$ we introduce variables $s=\sin V$ and $t=\sin Y$ and write Eq. (17) in the form

$$B_\perp(t) = \frac{1}{2\pi}\int_{-1}^{1}\frac{J(s)ds}{t-s}, \tag{B1}$$

where $B_\perp(t) = -\sin^{-1} t$ and $J(s) = 2\pi\sqrt{1-s^2}(d\varphi_0/ds)$. Clearly, Eq. (17) is the Biot-Savart integral for the normal component of the "field" $B_\perp(t)$ at the surface of a strip $-1<s<1$ carrying the "sheet current" $J(s)$. We, therefore, have to find $J(s)$ for a given $B_\perp(t)$. This problem is known to have a solution[31]

$$J(t) = \frac{2}{\pi}\int_{-1}^{1}\frac{B_\perp(s)ds}{s-t}\sqrt{\frac{1-s^2}{1-t^2}}. \tag{B2}$$

However, this solution is not unique because $J(s)$ is not determined by one field component. Currents of the form $C/\sqrt{1-s^2}$ with an arbitrary constant C correspond to $B_\perp=0$ and therefore can be added to Eq. (B2). This flexibility allows us to obtain φ_0' of the main text that satisfies boundary conditions [Eq. (15)].

APPENDIX C

The universal phase $\varphi_0(Y)$ is the solution of the linear integral equation [Eq. (15)] matching boundary conditions [Eq. (17)]. Numerically $\varphi_0(Y)$ can be obtained minimizing the functional

$$\mathcal{L} = \int_{-\pi/2}^{\pi/2}\int_{-\pi/2}^{\pi/2} dY d\tilde{Y}\varphi_0'(Y)\mathcal{F}(Y,\tilde{Y})\varphi_0'(\tilde{Y}) + \int_{-\pi/2}^{\pi/2} dY\left(Y^2 - \frac{\pi^2}{4}\right)\varphi_0'(Y), \tag{C1}$$

where

$$\mathcal{F}(Y,\tilde{Y}) = \frac{\cos\tilde{Y}}{\sin Y - \sin\tilde{Y}}. \tag{C2}$$

Minimization is done numerically using the finite element method.[32] We approximate the function $\varphi_0'(Y)$ by a finite set of basis functions v_i attached to a grid $Y_{i+1}=Y_i+\Delta$ with a constant Δ. Inside the interval $Y_{i-1}<Y<Y_{i+1}$, v_i is defined as

$$v_i = 1 - \frac{|Y-Y_i|}{\Delta} \tag{C3}$$

out of this interval $v_i=0$.

Next, we define a matrix

$$\mathcal{F}_{ij} = \int_{-\pi/2}^{\pi/2} \int_{-\pi/2}^{\pi/2} v_i(Y)\mathcal{F}(Y,\tilde{Y})v_j(\tilde{Y})dYd\tilde{Y} \qquad \text{(C4)}$$

and a vector

$$J_i = \int_{-\pi/2}^{\pi/2} v_i(Y)\left(Y^2 - \frac{\pi^2}{4}\right)dY. \qquad \text{(C5)}$$

Further, we approximate φ_0 and the functional $\mathcal{L}$ by

$$\varphi_0' \simeq \sum_i a_i v_i, \quad \mathcal{L} \simeq \sum_{i,j} a_i \mathcal{F}_{ij} a_j + \sum_i a_i J_i. \qquad \text{(C6)}$$

Clearly, $\mathcal{L}$ has a minimum at $a_i = \mathcal{F}_{ik}^{-1} J_k/2$. The universal solution $\varphi_0(Y)$ calculated using the finite elements method is shown in Fig. 2.

*mints@post.tau.ac.il

[1] Y. M. Ivanchenko and T. K. Soboleva, Phys. Lett. A **147**, 65 (1990); Y. M. Ivanchenko, Phys. Rev. B **52**, 79 (1995).
[2] P. A. Rosenthal, M. R. Beasley, K. Char, M. S. Colclough, and G. Zaharchuk, Appl. Phys. Lett. **59**, 3482 (1991).
[3] R. G. Mints and I. B. Snapiro, Phys. Rev. B **49**, 6188 (1994); **51**, 3054 (1995); **52**, 9691 (1995).
[4] Y. E. Kuzovlev and A. I. Lomtev, J. Exp. Theor. Phys. **84**, 986 (1997).
[5] V. G. Kogan, V. V. Dobrovitski, J. R. Clem, Y. Mawatari, and R. G. Mints, Phys. Rev. B **63**, 144501 (2001).
[6] A. A. Abdumalikov, Jr., M. V. Fistul, and A. V. Ustinov, Phys. Rev. B **72**, 144526 (2005).
[7] A. Gurevich, Phys. Rev. B **46**, 3187 (1992).
[8] M. Moshe, V. G. Kogan, and R. G. Mints, Phys. Rev. B **78**, 020510(R) (2008).
[9] J. Mannhart, H. Hilgenkamp, B. Mayer, C. Gerber, J. R. Kirtley, K. A. Moler, and M. Sigrist, Phys. Rev. Lett. **77**, 2782 (1996).
[10] D. J. Van Harlingen, Rev. Mod. Phys. **67**, 515 (1995).
[11] C. C. Tsuei and J. R. Kirtley, Rev. Mod. Phys. **72**, 969 (2000).
[12] H. Hilgenkamp and J. Mannhart, Rev. Mod. Phys. **74**, 485 (2002).
[13] A. A. Golubov, M. Yu. Kupriyanov, and E. Il'ichev, Rev. Mod. Phys. **76**, 411 (2004).
[14] R. G. Mints, Phys. Rev. B **57**, R3221 (1998).
[15] R. G. Mints, I. Papiashvili, J. R. Kirtley, H. Hilgenkamp, G. Hammerl, and J. Mannhart, Phys. Rev. Lett. **89**, 067004 (2002).
[16] H. J. H. Smilde, Ariando, D. H. A. Blank, G. J. Gerritsma, H. Hilgenkamp, and H. Rogalla, Phys. Rev. Lett. **88**, 057004 (2002).
[17] S. M. Frolov, D. J. Van Harlingen, V. V. Bolginov, V. A. Oboznov, and V. V. Ryazanov, Phys. Rev. B **74**, 020503(R) (2006).
[18] M. Weides, M. Kemmler, E. Goldobin, H. Kohlstedt, R. Waser, D. Koelle, and R. Kleiner, Phys. Rev. Lett. **97**, 247001 (2006).
[19] L. N. Bulaevskii, V. V. Kuzii, and A. A. Sobyanin, JETP Lett. **35**, 290 (1977).
[20] A. I. Buzdin, L. N. Bulaevskii, and S. V. Panjukov, JETP Lett. **25**, 178 (1982).
[21] A. I. Buzdin, Rev. Mod. Phys. **77**, 935 (2005).
[22] F. S. Bergeret, A. F. Volkov, and K. B. Efetov, Rev. Mod. Phys. **77**, 1321 (2005).
[23] A. Barone and G. Paterno, *Physics and Applications of the Josephson Effect* (Wiley, New York, 1982).
[24] M. Tinkham, *Introduction to Superconductivity*, 2nd ed. (Dover, New York, 2004).
[25] P. M. Morse and H. Feshbach, *Methods of Theoretical Physics* (McGraw-Hill, New York, 1953), Vol. 2, Chap. 10.
[26] V. G. Kogan, J. R. Clem, and R. G. Mints, Phys. Rev. B **69**, 064516 (2004).
[27] G. Stan, S. B. Field, and J. M. Martinis, Phys. Rev. Lett. **92**, 097003 (2004).
[28] E. Bronson, M. P. Gelfand, and S. B. Field, Phys. Rev. B **73**, 144501 (2006).
[29] K. H. Kuit, J. R. Kirtley, W. van der Veur, C. G. Molenaar, F. J. G. Roesthuis, A. G. P. Troeman, J. R. Clem, H. Hilgenkamp, H. Rogalla, and J. Flokstra, Phys. Rev. B **77**, 134504 (2008).
[30] R. G. Mints and V. G. Kogan, Phys. Rev. B **55**, R8682 (1997).
[31] E. H. Brandt, Phys. Rev. B **46**, 8628 (1992).
[32] G. Strang and G. Fix, *An Analysis of the Finite Element Method*, 2nd ed. (Wellesley, Cambridge, 2008).